



# 1 Shaping shallow landslide susceptibility as a function of 2 rainfall events

3 Micol Fumagalli<sup>1</sup>, Alberto Previati<sup>1</sup>, Paolo Frattini<sup>1</sup>, Giovanni B. Crosta<sup>1</sup>

4 Department of Earth and Environmental Sciences, University of Milano-Bicocca, Piazza della Scienza 4, 20126 Milano, Italy

5 *Correspondence to:* Micol Fumagalli (m.fumagalli86@campus.unimib.it)

6 **Abstract.** This paper tests a multivariate statistical model to simulate rainfall dependent susceptibility scenarios of shallow  
7 landslides. To this end, extreme rainfall events spanning from 1977 to 2021 in the Orba basin (a study area of 505 km<sup>2</sup> located  
8 in Piedmont, northern Italy), have been considered. First of all, the role of conditioning and triggering factors on the spatial  
9 pattern of shallow landslides in areas with complex geological conditions is analysed by comparing their spatial distribution  
10 and their influence within logistic regression models, with results showing that rainfall and specific lithological and  
11 geomorphological conditions exert the strongest control on the spatial pattern of landslide.  
12 Different rainfall-based scenarios were then modelled using logistic regression models trained on different combinations of  
13 past events and evaluated using an ensemble of performance metrics. Models calibrated on multi-events outperform the ones  
14 based on a single event, since they are capable of compensating for local misleading effects that can arise from the use of a  
15 single rainfall event. The best performing developed model considers all the landslide triggering rainfall scenarios and two  
16 non-triggering intense rainfall events, with a score of 0.90 out of 1 on the multi-criteria TOPSIS-based performance index.  
17 Finally, a new approach based on misclassification costs is proposed to account for false negatives and false positives in the  
18 predicted susceptibility maps.  
19 Overall, this approach based on a multi-event calibration and on a misclassification costs analysis shows promise in producing  
20 rainfall dependent shallow landslide susceptibility scenarios that could be used for hazard analyses, early warning systems and  
21 to assist decision-makers in developing risk mitigation strategies.

## 22 1 Introduction

23 Shallow landslides are a widespread phenomenon that affects many regions of the world (Petley, 2012). In Italy, according to  
24 the last national report on landslides and floods, almost 8% of the country is affected by landslides, of which 15% are classified  
25 as rapid flow and 6% as shallow landslides (ISPRA, 2021). According to Cruden and Varnes (1996), these are shallow slides,  
26 mainly translational, with a thickness ranging between 0.5 and 2 m (Bandis et al., 1996; Mason and Rosenbaum, 2002). Shallow  
27 landslides are generally triggered by rainfall events, which cause an increase in pore water pressure, or a loss of apparent  
28 cohesion generated by suction (Caine, 1980; Crosta and Frattini, 2003; Fredlund et al., 1978; Iverson, 2000; Lu and Godt,



29 2008). Despite their limited initial volume, these landslides may be characterized by a high density per unit area and can evolve  
30 in debris flows. The high velocity and the difficulty of prediction due to the almost complete lack of premonitory signs  
31 (Campbell, 1975; Frattini et al., 2009; Montrasio et al., 2016) make these phenomena seriously dangerous in terms of life and  
32 economic losses (Trigila and Iadanza, 2012).

33 A common definition of landslide hazard is “the probability of occurrence within a specific period of time and within a given  
34 area of potentially damaging phenomena” (Varnes, 1984), requiring the quantification of the magnitude, the spatial and the  
35 temporal probability for an instability event to occur. The variables that control landslide hazard are commonly distinguished  
36 into conditioning and triggering factors. Conditioning factors are generally assumed to have no temporal dependence and are  
37 responsible for “where” a landslide might occur, while triggering factors are event-related and control “when” a landslide might  
38 occur (Crosta and Frattini, 2003; Lombardo et al., 2020; Wu and Sidle, 1995), although their spatial properties (e.g. distribution  
39 of intensity or cumulative rainfall during a rain event) play a key role in determining the location of landslides.

40 The spatial likelihood of shallow landslide occurrence is addressed through landslide susceptibility models, based on either  
41 physically based or machine-learning techniques. Physically based techniques for shallow landslides often combine the  
42 infinite-slope model with hydrogeological models, which require many different input data; for this reason, they are more  
43 frequently applied at the site-scale (Baum et al., 2008; Montgomery and Dietrich, 1994).

44 Machine-learning methods search for functional relationships between the conditioning factors and the distribution of  
45 landslides, obtained from inventories of past events (Carrara, 1983; Goetz et al., 2015; Huang et al., 2020; Reichenbach et al.,  
46 2018; van Westen et al., 2008). Susceptibility models are usually considered as time-independent, meaning that the likelihood  
47 of landslides occurrence does not vary in time (Jones et al., 2021; Lombardo et al., 2020). However, many authors demonstrated  
48 that this assumption is often violated both on a long (hundreds or thousands of years) and on a short timescale (tens of years),  
49 especially in view of climate changes (Hungr, 2016; Samia et al., 2018). The “when” problem has typically been addressed by  
50 using rainfall thresholds or Physically based models. Rainfall thresholds describe the rainfall intensity, duration or cumulative  
51 event precipitation that may trigger landslides for a particular area (Caine, 1980; Crosta, 1998; Guzzetti et al., 2007). This  
52 approach has usually disregarded soil features and morphometric conditioning factors, such as the geotechnical features of the  
53 involved materials, until recent times, when hydrogeological effects started to be included into the analyses, for example  
54 through the consideration of the soil water content prior to the triggering event (Bogaard and Greco, 2018; Marino et al.,  
55 2020a). Some authors started testing approaches to address both the “where” and the “when” questions in the context of early  
56 warning systems. For example, Kirschbaum and Stanley (2018), used a fuzzy overlay model to combine static explanatory  
57 variables into a susceptibility map. This information was then incorporated into a heuristic decision tree model together with  
58 dynamic variables such as antecedent precipitation, giving a model capable of indicating potential landslide activity in near  
59 real-time. Segoni *et al.* (2018b), combined rainfall thresholds and susceptibility maps into a hazard matrix, while Bordoni *et al.*  
60 *et al.* (2021), integrated rainfall thresholds and antecedent soil humidity with a susceptibility model in order to forecast the spatial  
61 and temporal probability occurrence of shallow landslides. Camera *et al.* (2021) included intense rainfall and snowmelt in a  
62 landslide susceptibility model trained over multiple landslide inventories and different meteorological conditions, making it



63 potentially more robust to investigate the effects of climate changes. Knevels *et al.* (2020) and Maraun *et al.* (2022), included  
64 5 days cumulated rainfall and maximum 3 hours rainfall intensity to model landslides associated with an extreme rainfall event,  
65 and then applied their findings to an event storyline approach to analyse the future landslide occurrence probability under  
66 climate changes. Moreno *et al.* (2024) integrated static and time-dependent controlling factors into a generalized additive  
67 mixed model (GAMM) model to forecast shallow landslides in space and time, showing that both short-term (2 days) and  
68 medium-term (14 days) cumulative precipitation increases the model capabilities.

69 Yet, the integration of static and time-varying factors into machine-learning models still remains challenging, but it could  
70 become a powerful instrument to better understand the connection between a variation in the time-dependent controlling factors  
71 and landslide triggering, thus helping at improving landslide prediction in a changing climate.

72 An important issue for the application of susceptibility models is the evaluation of their performance. For models that predict  
73 binary stable and unstable slopes it is necessary to choose a cut-off value below which the predicted susceptibility values are  
74 treated as 0 and above which the values are treated as 1 (Beguería, 2006; Brenning, 2005; Frattini *et al.*, 2010; Goetz *et al.*,  
75 2015; Guzzetti *et al.*, 1999). This results in a contingency matrix quantifying the total number of correctly and incorrectly  
76 classified units. From this matrix, it is possible to assess the performance by using several performance statistics, such as the  
77 Accuracy (i.e. the ratio between the correctly classified samples and the total number of samples), the Precision (i.e., the ratio  
78 between the true positive samples and all the positively classified samples), the True Positive Rate TPR (i.e., the ratio between  
79 the true positive and all the positives), the False Positive Rate FPR (i.e., the ratio between the false positives and all the  
80 negatives), the Threat score (Gilbert, 1884), the Pierce's skill score (True skill statistic; Peirce, 1884), the Heidke's skill score  
81 (Cohen's kappa; Heidke, 1926), and the odd ratio skill score (Yule's Q; Yule, 1900).

82 However, the choice of the cut-off value is a complex problem, and therefore the performance is frequently evaluated by using  
83 cutoff-independent methods, such as the Receiver Operating Characteristic (ROC) curves (Frattini *et al.*, 2010; Hosmer and  
84 Lemeshow, 2000; Provost and Fawcett, 2001) or the Precision-Recall (PR) curves (Davis and Goadrich, 2006; Raghavan *et al.*,  
85 1989; Saito and Rehmsmeier, 2015). The ROC curve represents the FPR and TPR obtained for different cutoffs. The Area  
86 Under the Curve (AUROC) can be used to quantify the overall quality of the model (Hanley and McNeil, 1982). However,  
87 ROC curves can overestimate the performance of a model when the distribution of the input classes is highly skewed. For this  
88 reason, the Precision-Recall (PR) curves have also been used (Nam *et al.*, 2024; Yordanov and Brovelli, 2020; Zhao *et al.*,  
89 2022), which plots the precision (i.e., the proportion of true positives among the positive predictions) against the TPR.  
90 However, unlike ROC curve, the value under the PR curve is not directly interpretable for model evaluation, especially because  
91 of a non-universal baseline performance, which depends on the class distribution, and a non-linear interpolation of precision  
92 values. Nevertheless, PR analysis can be adapted to be used similarly to the ROC analysis by using Precision-Recall-Gain  
93 curves (PRG), which make use of the F-Gain score, a linearized version of the  $F_1$  score, to properly take baselines into account  
94 (Flach and Kull, 2015). In landslides-related problems, the quantification of the costs linked to the use of a model is also an  
95 important issue. Therefore, the performance of the model can be done with an approach that minimize the expected



96 misclassification costs, through the cost curves (Drummond and Holte, 2006; Frattini et al., 2010). Moreover, the cost curve  
97 allows to identify the optimal cut-off to be used for the performance evaluation.

98 A multivariate statistical analysis for the Piedmont area of the Orba basin (northern Italy) has been developed in this paper,  
99 considering rainfall scenarios spanning from 1977 to 2021, to investigate the correlation between landslides distribution and  
100 the spatial pattern of conditioning and triggering factors. Different logistic regression models were trained for different  
101 landslides and rainfall scenarios, and their performance was evaluated through an ensemble of performance metrics, leading  
102 to an optimal choice of the best model for scenario-based problems or early warning.

103 This work allows to address the following research questions:

- 104 • To what extent the pattern of shallow landslides is controlled by the characteristics of the rainfall event in areas with  
105 complex geological conditions?
- 106 • How can rainfall be used within a statistical model to produce instability scenarios for different rainfall events?
- 107 • Which is the best strategy to train a statistical model based on an ensemble of rainfall events?
- 108 • Which is the most significant classification scheme to produce a susceptibility map for early warning purposes?

109 The novelty of this work lies in the definition of a critical selection strategy of the optimal ensemble of rainfall events to  
110 produce a susceptibility map that may be helpful for scenario-based problems and early warning purposes. Moreover, a new  
111 methodology is proposed for the classification of the regression results, used for the realization of the final resulting maps.

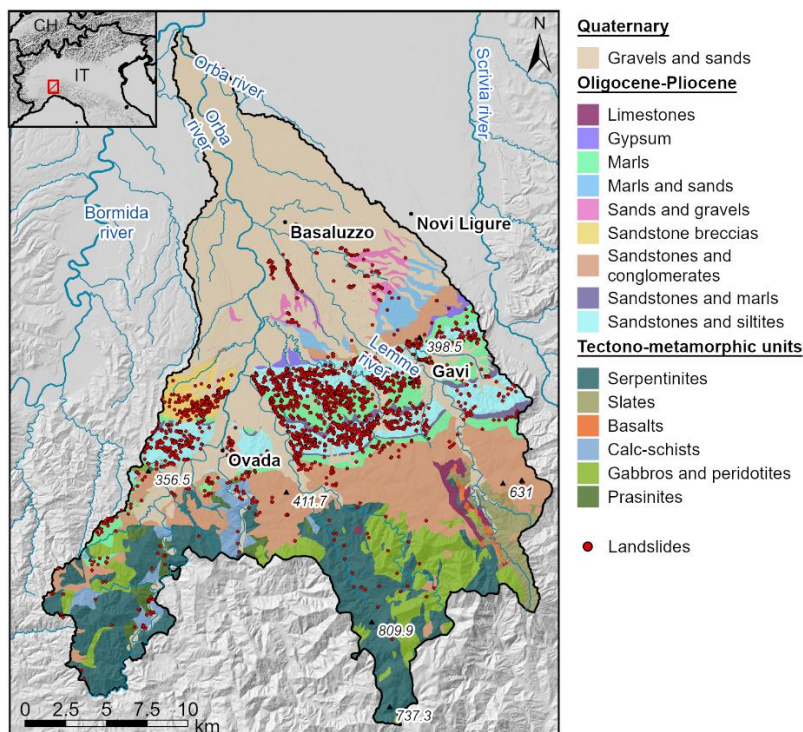
## 112 **2 Materials and methods**

### 113 **2.1 Study area**

114 The Orba basin is located in the Langhe and Monferrato Hills of Piedmont Region, north-western Italy. This area has been  
115 affected by several high-magnitude floods and severe slope instabilities during the last century, caused by intense rainfall  
116 events (Mandarino et al., 2021). The study area has an extension of 505 km<sup>2</sup> and it is situated between 80 and 1170 m a.s.l.  
117 The main river of the basin, the Orba River, flows northward from the Ligurian Apennines to the confluence with the Bormida  
118 River, a right tributary of the Po River. The study area overlaps metamorphic lithotypes in the southern part – mainly  
119 peridotites, serpentinites and serpentine-schists, meta-gabbros and meta-sediments belonging to the Voltri Massif and the  
120 Sestri-Voltaggio Zone (Piana et al., 2017) – while in the central part of the area the sedimentary sequence of the Tertiary  
121 Piedmont Basin (TPB) outcrops. The TPB evolved from the Late Eocene to the Late Miocene over the inner part of the Alpine  
122 wedge (Coletti et al., 2015) and is mainly represented in the area by conglomerates, sandstones and marls. The northern sector  
123 of the basin presents quaternary fluvial deposits belonging to the Alessandria – Tortona floodplain. The morphology of the  
124 area is strongly controlled by the TPB sedimentary succession: where the strata are harder, the landscape presents hilly reliefs  
125 dipping in the same direction as the underlying layers, while lowered areas modelled by fluvial erosion are present where the  
126 lithologies are more erodible. When the dipping of the strata becomes gentler, the morphology becomes more uniform and



127 characterized by a dense hydrographic network. The mean annual temperature is 13° and the average annual precipitation  
128 ranges from around 600 mm/year in the northern part to 1600 mm/year in the southern part, with autumn as the rainiest season  
129 (Fioravanti et al., 2022; Luino, 2005). Land use is primarily forest (45%), with crops and meadows (24%) near the confluence  
130 with the Po River.



131  
132 **Figure 1. Location of the Orba basin, with the spatial distribution of shallow landslide observed in three different events, and with**  
133 **the main lithologies.**

## 134 2.2 Data

### 135 2.2.1 Rainfall events and landslide inventories

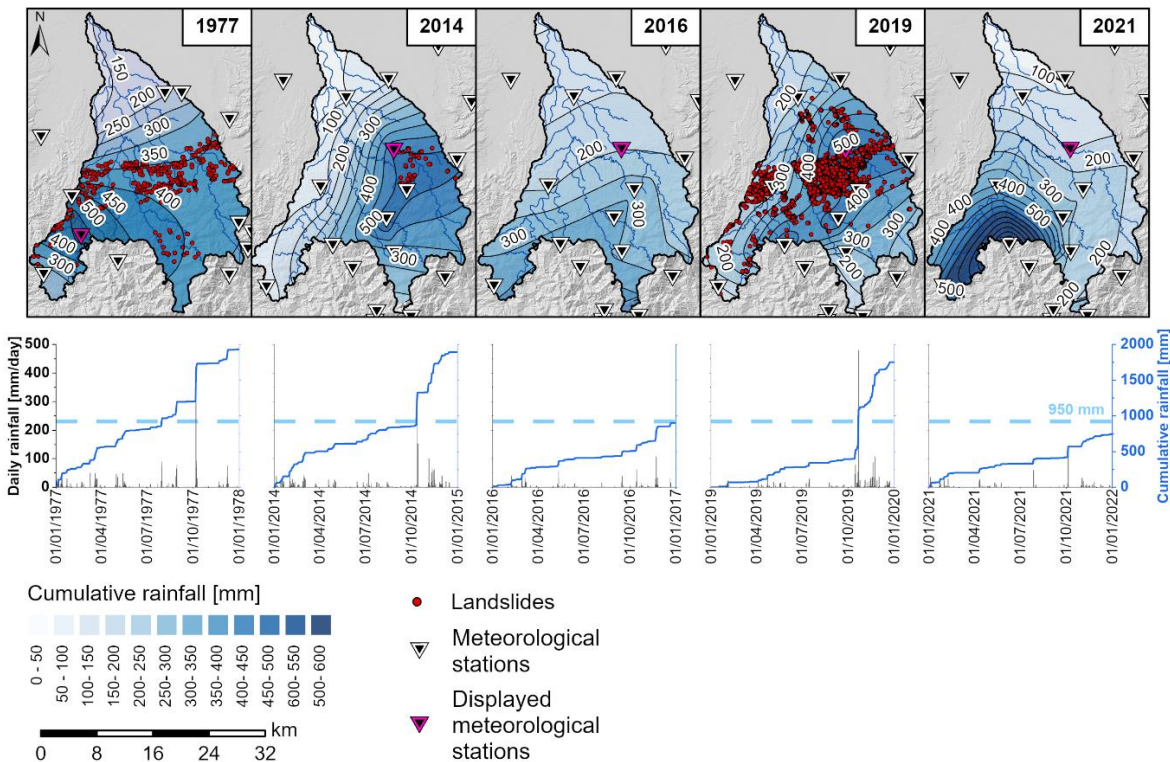
136 Three landslide inventories were compiled for three recent extreme rainfall events (1977, 2014 and 2019) through the analysis  
137 of Google Earth images, national and regional orthophotos, published event maps, and field reconnaissance (Fig. 1). Part of  
138 the inventories was already available online (SIFRAP, Sistema Informativo sulle FRane in Piemonte), while the most recent  
139 event was provided for this project by the Regional Environmental Protection Agency of Piedmont (ARPA Piemonte, personal  
140 communication). The 2014 and 2019 inventories include polygons of each single shallow landslide, while the 1977 inventory  
141 represents clusters of shallow landslides as polygons. However, this difference is negligible when choosing slope units as  
142 mapping units for the analyses (Sect. 2.3).

143 The first shallow landslide event was triggered by heavy rainfall at the beginning of October 1977. Between October 6<sup>th</sup> and  
144 7<sup>th</sup>, more than 400 mm of rain fell in less than 24 hours, causing flooding, bank and riverbed erosion, debris flows and soil



145 slips (INTERREG IIC, 1998)(Fig. 2). The second shallow landslide event was triggered in October 2014 with more than 420  
146 mm of rain in less than 12 hours, as recorded at the Gavi meteorological station on October 13<sup>th</sup>(Fig. 2), for which the mean  
147 annual total rainfall is 1000 mm (calculated for the 1991 – 2020 time interval, ARPA Piemonte). The third shallow landslide  
148 event occurred in late October 2019. In the afternoon and evening of October 21<sup>st</sup> more than 400 mm of rain (Gavi station) fell  
149 in less than 12 hours, resulting in a very high-magnitude flood and widespread shallow landslides (ARPA Piemonte, 2019)  
150 (Fig. 2).

151 In addition to these three landslide-triggering rainfall events, two intense precipitation events (2016 and 2021) that were not  
152 associated to landslides were selected, in order to test the capabilities of the models to discriminate between triggering and  
153 non-triggering rainfall characteristics. The 2016 event hit the Piedmont region with strong and persistent rainfalls between  
154 November 21<sup>st</sup> and 25<sup>th</sup>, and triggered almost 1000 landslides, none of which in the Orba basin. Indeed, the peak of the  
155 cumulative precipitation was localized more southward compared to the ones previously described, with up to 400 mm of rain  
156 in the southern edge of the Orba basin (Fig. 2). The other event happened from October 3<sup>rd</sup> to 5<sup>th</sup>, 2021. The Ligurian-Piedmont  
157 watershed was the most affected area, with a peak of 472 mm of rain in 12 hours recorded in the south-western part of the  
158 area. The total precipitation in the Orba basin was up to 750 mm in the south-western edge of the basin (Fig. 2).



159  
160 **Figure 2. Rainfall and landslides distribution during the considered events, reconstructed by interpolation of values measured by**  
161 **the meteorological stations on the ground, that led to landslide triggering in the Orba basin. Graphs report the daily and cumulative**  
162 **rainfall for the year in which the shallow landslides were triggered are shown. Dashed lines represent the mean annual rainfall for**  
163 **the basin of interest (ARPA Piemonte).**



164 For all the inventories, a non-cumulative logarithmic binned landslide size probability density distribution was developed as:

$$165 \quad p(A) = \frac{1}{N_{tot}} \frac{\partial N}{\partial A} \quad (1)$$

166 where  $\partial N$  is the number of landslides with an area between  $A$  and  $A + \partial A$  and  $N_{tot}$  is the total number of landslides within a  
 167 study area (Malamud et al., 2004). Following (Frattini and Crosta, 2013), a Pareto distribution was fitted to the probability  
 168 density above a minimum size cut-off with (Fig. 3):

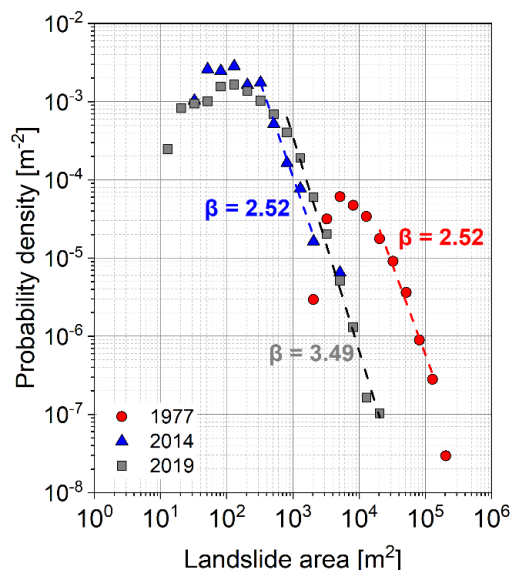
$$169 \quad p(A) = \alpha c^\alpha A^{-\alpha-1} \quad c > 0, \quad \alpha > 0, \quad A \in [c, \infty) \quad (2)$$

170 Using the maximum likelihood estimation, the distribution parameters were estimated, obtaining a good fitting for landslides  
 171 larger than  $500 \text{ m}^2$ , with the best fitting results for landslides greater than  $1000 \text{ m}^2$ . The scaling exponents  $\alpha$  vary between 1.5  
 172 and 2.6, values that are higher than most of those reported in literature but still in the range (Van Den Eeckhaut et al., 2007).

173

174 **Table 1. Statistical parameters describing the landslide events in the study area.**

Event	Number	Density %	Total landslide area [ $\text{km}^2$ ]	Mean landslide area [ $\text{m}^2$ ]
6 – 7 October 1977	366	1.31	7.82	21373
9 – 13 October 2014	66	0.004	0.023	353
19 – 22 October 2019	2088	0.26	1.57	124



175

176 **Figure 3. Probability density – areas distribution of the shallow landslides for the three events within the study area. As stated in the**  
 177 **main text, the 1977 landslide inventory shows a different distribution, shifted to the right, because of the different chosen mapping**  
 178 **criteria. Power-law fitting with maximum likely estimator is reported ( $\beta = -\alpha-1$ ).**



## 179 2.2.2 Landslide conditioning and triggering factors

180 The conditioning factors used in the following analyses include 7 morphometric parameters, lithology, soil grain size  
181 distribution, and land use (Fig. S1). The morphometric parameters were extracted from a 5m resolution DEM provided by  
182 Piedmont region. The morphometric factors are slope angle, northerness, easternness, profile curvature, planar curvature, total  
183 curvature, and flow accumulation. Lithological information was obtained from the geological map of Piemonte Region, at  
184 scale 1:250,000 (Piana et al., 2017). The units have been reclassified by aggregating geo-stratigraphic units with comparable  
185 lithological and litho-technical characteristics, resulting in 16 lithological classes (Fig.1: gravels and sands, limestones,  
186 gypsum, marls, marls and sands, sands and gravels, sandstone breccias, sandstones and conglomerates, sandstones and marls,  
187 sandstones and siltites, serpentinites, slates, basalts, calcschists, gabbros and peridotites, and prasinites).

188 Information relative to the soils grain size distribution was retrieved from the SoilGrids maps (Poggio et al., 2021), reporting  
189 soil properties for the entire globe with a resolution of 250 m. SoilGrids models were obtained through the application of  
190 machine learning to soil data collected worldwide.

191 The land use was obtained from the 10 m resolution LAND COVER PIEMONTE map, which integrates information collected  
192 between 2018 and 2022 (<https://geoportale.igr.piemonte.it/cms/progetti/land-cover-piemonte>, last access 21/10/2023). 12  
193 different land use classes were used, namely arable land, areas with sparse/absent vegetation, artificial non-agricultural green  
194 areas, heterogeneous agricultural areas, inland waters, mining areas, permanent crops, permanent lawns, road network,  
195 shrubby/herbaceous areas, urbanized and productive areas, and woods.

196 Besides the predisposing factors, several rainfall parameters potentially responsible for the shallow landslides triggering were  
197 also included into the analysis. These parameters were obtained by interpolating daily rainfall data collected at 39 and 51  
198 gauging stations for the 1977 and 2014/2019 rainfall events, respectively. In particular, the maximum daily rainfall intensity  
199 (mm/day), the total rainfall of the events (Table 1), and the antecedent cumulative rainfall (mm) over 10, 30, 60 and 90 days  
200 (Smith et al., 2023) as a proxy of soil water content prior to the event (Guzzetti et al., 2007), which can increase the likelihood  
201 of failure (Bogaard and Greco, 2018; Thomas et al., 2018), were extracted. Maximum daily rainfall intensities were normalized  
202 by the daily rainfall with a return period of 10 years, provided by ARPA Piemonte with a grid resolution of 250 m, while the  
203 total and antecedent rainfall values were normalized by the mean annual precipitation (1991 – 2020) within the study areas.  
204 Data normalization was performed because previous studies (Marc et al., 2019; Smith et al., 2023) found that the spatial pattern  
205 of shallow landslides is more correlated with rainfall anomalies rather than with rainfall absolute values.

206 A correlation analysis between these rainfall variables revealed a strong linear correlation between the maximum rainfall  
207 intensity and the total rainfall of the event – probably due to the coarse temporal aggregation used to estimate the maximum  
208 intensities. A strong correlation was also found between the antecedent cumulative values over different aggregation time  
209 windows. For the subsequent regression analyses, an a priori selection was made to extract the two most influencing rainfall  
210 variables: the maximum daily rainfall intensity as an intra-event descriptor, and the 90-day cumulative rainfall for the  
211 antecedent condition. The latter was selected by testing the correlation between the cumulative rainfall values and the soil





212 humidity obtained from the ERA5-Land dataset (ERA5-Land hourly data from 1950 to present.; Hersbach et al., 2020; Muñoz-  
213 Sabater et al., 2021), from which the highest correlation was found when using a time window of 90 days (Fig. S2).

### 214 **2.3 Slope unit delineation**

215 The application of statistical models to landslide susceptibility zoning requires the partition of the study area in terrain units,  
216 such as unique condition units, slope units, grid-cells, or others (Carrara et al., 1991, 2008). Among these, slope units were  
217 chosen since they provide several advantages, such as: (i) the high geomorphological meaning of the terrain unit; (ii) the  
218 possibility to use continuous values (i.e. percentage within the unit) for the categorical variables, rather than binary values  
219 (Carrara *et al.*, 1991), (iii) an efficient handling of possible mapping uncertainties, thanks to the generalization of the  
220 predisposing factors falling within them (Jacobs et al., 2020; Steger et al., 2016). Their delineation is based on the identification  
221 of drainage and divide lines, and was done automatically by using the *r.slopeunits* algorithm (Alvioli et al., 2016). This iterative  
222 algorithm requires as input data the minimum circular variance for each unit, representing the allowed variability of orientation  
223 for each grid cell belonging to the same unit, and the minimum area for each slope unit.

### 224 **2.4 Preliminary exploratory statistical analysis**

225 To understand which variables exert the strongest control on the landslide distribution, and if this control remains constant  
226 through time, the distributions of the mean values of each covariate for the slope units affected by shallow landslides were  
227 compared with the same distributions for the whole study area, and for the other inventories. The similarity among the  
228 inventories for each covariate (i.e., the null hypothesis) is rejected if the p-value of the Dunn's test is smaller than 0.05.

229 To further investigate the role of antecedent and triggering precipitation, the relationship between landslide density (i.e., total  
230 landslide area over the total slope units area) and precipitation classes (i.e., normalized maximum rainfall intensity, normalized  
231 cumulative rainfall, and normalized antecedent cumulative rainfall) was analysed through the Spearman's rank order  
232 correlation coefficient. Given the strong lithological control, the analysis was conducted for the entire study area and separately  
233 for the most unstable lithological units (marls – around 30% of the total landslides number of each event, sandstones and  
234 siltites – almost 50% of landslide in each event, sandstone breccias – 7% of landslides in 1977 and 2019, 0% in 2014, and  
235 sandstones and marls – 4% in 1977 and 2019, 14% in 2014).

### 236 **2.5 Rainfall-based susceptibility analysis**

237 Binary logistic regression was chosen for the susceptibility analysis because of its widespread and validated use and because  
238 it provides the importance of each conditioning variable in terms of standardized regression coefficients in a straightforward  
239 manner (Carrara, 1983; Micheletti et al., 2015; Reichenbach et al., 2018).

240 Logistic regression describes the relationship between a binary outcome (stable or unstable unit) and a set of independent  
241 variables (Hosmer and Lemeshow, 2000). The probability  $p$  of a sample to belong to a certain group is given by:



$$242 \quad \ln \frac{p}{1-p} = B_0 + B_1 X_1 + B_2 X_2 + B_3 X_3 + \dots + B_m X_m \quad (3)$$

243 where  $B_i$  are the logistic coefficients, estimated from the data, that quantify the contribution of each variable  $X_i$  to the final  
244 outcome. Logistic regression assumes that a linear relationship exists between the logit transformation of the binary outcome  
245 and each variable selected by the model through a forward stepwise method, with a variable being included into the model if  
246 the probability of its score statistics is smaller than an entry value of 0.05, and being removed if the probability is greater than  
247 a removal value of 0.10. Before running the models, variables showing a strongly skewed distribution were normalized using  
248 a log-transformation (Carrara et al., 2008), and all the static variables were then standardized using a z-score normalization  
249 (mean equal to 0 and standard deviation equal to 1), in order to make their estimated regression coefficients comparable  
250 (Lombardo and Mai, 2018).

251 Five susceptibility models were developed. Models m77, m14 and m19 were trained on a single landslide event (i.e., 1977,  
252 2014, and 2019, respectively). The model m771419 was trained by merging all the landslide events, and finally the model  
253 m7714161921 was trained by merging different rainfall events with or without landslides. Each dataset was divided into  
254 training (3/4) and validation (1/4) subsets, the former being used to build the models and the latter to evaluate their predictive  
255 performance. Each model was evaluated against itself and against all the other landslide events by using cross-validation.  
256 Model evaluation was performed with the following strategy. First of all, two common cut-off independent methods were  
257 applied (ROC and Precision Recall Gained (PRG) curves) to obtain their Area Under Curves. Then, the optimal cut-off  
258 obtained by the ROC analysis was used to derive the optimal contingency matrix, from which the accuracy, precision, TPR  
259 and FPR were calculated. Finally, these indices were summed up with a multiple attribute decision making procedure,  
260 performed with the technique for order preference by similarity to ideal solution (TOPSIS, Hwang and Yoon, 2012), to  
261 individuate the best model. For each model, 50 logistic regression analyses were run, in order to statistically analyse the  
262 distribution of the susceptibility values, the regression coefficients, and the performance metrics.

263 To avoid an over-abundance of obviously stable units (e.g., flat areas), which would give a biased estimate of the performance,  
264 only nontrivial units with slopes more compatible with shallow landslides triggering ( $>20^\circ$  and  $<$  than  $40^\circ$ ) were selected.

265 The economic consequences are one of the main issues in early warning; these economic costs can be significantly different  
266 in case of false or missing alarms. This problem is usually not considered in susceptibility studies, where the classification of  
267 susceptibility into classes (e.g. very low, low, medium, high and very high) is based on some arbitrary choice of the modeler  
268 (Cantarino et al., 2019).

269 For this reason, a new practical approach to classify the susceptibility values was defined, based on the cost-curves approach.  
270 Similarly to other methods, such as Natural Breaks (Jenks, 1967), this procedure takes into account the underlying data, instead  
271 of using standard classes, with the advantage that it can be calibrated on a specific cost analysis.

272 Specifically, the cut-off corresponding to the minimum normalized expected cost was used as the centre of the third class  
273 (medium susceptibility), and defined in this work as *half-susceptibility threshold (HST)*. The classes limits are defined based  
274 on a geometric progression from 0 to 1, centred on HST.



275 Since the misclassification costs can vary significantly within the study area, and their quantification require extremely detailed  
276 analyses, in the current work the a priori probabilities of having and not having landslides were kept equal, while three  
277 scenarios of relative costs (Scenario 1:  $c(-|+):c(+|-) = 0.5 : 0.5$ , Scenario 2:  $c(-|+):c(+|-) = 0.8 : 0.2$ , Scenario 3:  
278  $c(-|+):c(+|-) = 0.2 : 0.8$ , where  $c(-|+)$  is the cost of false negatives and  $c(+|-)$  is the cost of false positives) were  
279 considered.

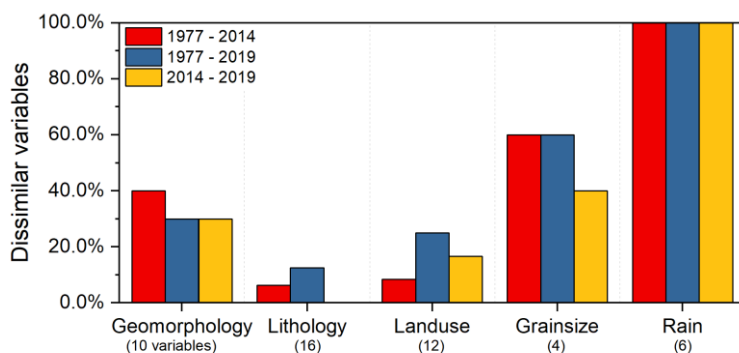
## 280 3 Results

### 281 3.1 Slope units delineation

282 By using a minimum area of 20,000 m<sup>2</sup> and a maximum circular variance of 0.1, the study area was partitioned in 10'528 slope  
283 units, with an average area of 56'555 m<sup>2</sup> and a maximum area of 1'868'299 m<sup>2</sup>. Slope units were classified as unstable if  
284 occupied by at least one landslide. This resulted in 627 (5.95%), 50 (0.47%), and 869 (8.25%) unstable slope units for the  
285 1977, 2014, and 2019 events, respectively.

### 286 3.2 Preliminary exploratory statistical analysis

287 Figure 4 represents the percentage of variables within the different groups of controlling factors for which the similarity  
288 hypothesis between the variable distributions in the unstable slope units for the different inventories can be rejected (see Fig.  
289 S3 for all the distributions). Lithological variables show the lowest dissimilarity between the different inventories, followed  
290 by land use. On the other side, the rainfall variables are always dissimilar among the inventories. This suggests that landslides  
291 may be triggered by different rainfall patterns, but within certain specific lithological and land use classes.



292

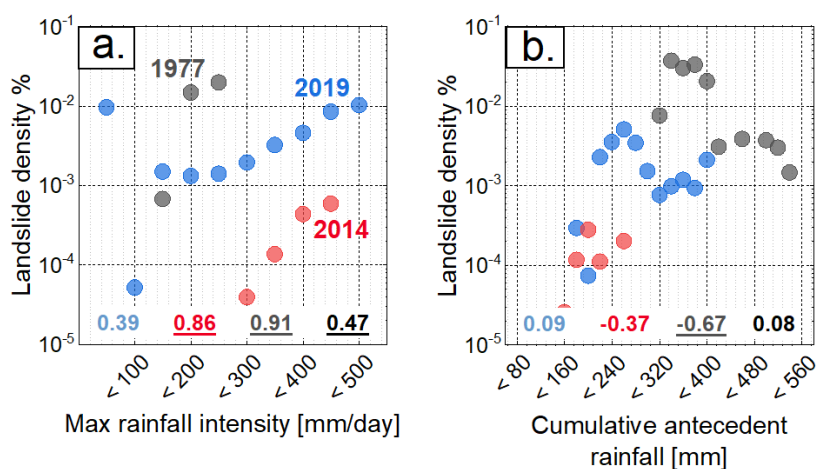
293 **Figure 4. Percentage of statistically dissimilar variables within each group of controlling factors, according to the Dunn's test with**  
294 **a significance level of 0.05.**

295 To further investigate the control of rainfall on landslide triggering, landslide density was plotted against classes of maximum  
296 rainfall intensity, cumulative rainfall during the event and 90 days antecedent cumulative rainfall (Fig. 5).



297 Firstly, the three landslide events show significant differences, confirming the previous results. Considering the whole study  
298 area, landslide density is clearly positively correlated with maximum rainfall intensity during the event. Interestingly, for the  
299 same maximum rainfall intensity (Fig. 5a), the landslide density is offset for the three inventories, indicating a different  
300 sensitivity of landslides to rainfall. This could be explained by the different levels of antecedent rainfall (Fig. 5b): the higher  
301 the antecedent cumulative rainfall, the higher the sensitivity.

302 The same analysis for individual lithologies did not show clear evidences, probably due to the smaller sample of landslides in  
303 each class (Fig. S4). This is more evident for sandstones and breccias, as this lithology is restricted to a relatively small sector  
304 in the western part of the study area.



305  
306 **Figure 5. Scatterplots representing landslide density in each rainfall class for the entire study area. Spearman's rank order**  
307 **correlation coefficients between landslide density and rainfall classes are reported in each plot. Underlined values are statistically**  
308 **correlated at the 0.05 level.**

309 For the 1977 and 2019 events, Fig. 5a shows that landslides started to occur for maximum rainfall intensities greater than 100  
310 mm in 24 h, which agrees with the ID curves proposed for the area (Tiranti et al., 2019). On the other hand, during the 2014  
311 event, a rainfall intensity of 250 mm in 24 hours was necessary to cause instabilities. This may be explained by looking at the  
312 cumulative antecedent rainfall in 90 days, which is below 300 mm in 2014, and much higher for the other events, giving  
313 different initial soil moisture conditions.

314 Also, all the three inventories show a positive correlation between the landslide density and the normalized maximum rainfall  
315 intensity over 24 hours. On the contrary, the values of antecedent and intra-event cumulative rainfall are significantly different  
316 between the three events (Fig. 4), as confirmed by Fig. 5. Moreover, the different average levels of antecedent conditions,  
317 whose pattern is not spatially correlated with the distribution of maximum intensity, also play a role in offsetting the  
318 relationship between landslide density and the maximum rainfall intensity. Figure 5 shows that landslide density increases  
319 more rapidly with rainfall as a function of the initial conditions (for example, landslide density for 400 mm is  $4.36e^{-4}$  for the  
320 2014 event, and  $4.65e^{-3}$  for 2019).



### 321 3.3 Rainfall based susceptibility maps

322 Figure 6 shows the mean coefficient and the inclusion rate of the 50 runs of the logistic regression models, for each single  
323 variable. Slope gradient is the most important parameter for all models (except m14), with always positive coefficients and a  
324 high inclusion rate. For the other morphometric parameters, northerness and flow accumulation show a high inclusion rate and  
325 relatively high coefficients (except for m14). The negative sign of the northerness coefficient indicates the south-facing slope  
326 units as more unstable. Among the lithological descriptors, “gravels and sands”, “sandstones and siltites”, and “marls” show  
327 the highest inclusion rates and coefficient values. On the other end, basalts, limestones, and slates are never included in the  
328 models. Land use does not exert an important control. Among the descriptors of soil granulometry, the contents in coarse  
329 fragments and sand are selected with a high inclusion rate and a negative median coefficient, with the exception of m14, while  
330 clay content is chosen with a high inclusion rate and a positive median coefficient.

331 Eventually, rainfall variables play an important but complex role on susceptibility. Maximum daily intensity is very important  
332 for m14, m771419, and m7714161921, with positive coefficients and a high inclusion rate. Surprisingly, maximum rainfall  
333 intensity is not included in m19, and takes negative values in m77. The antecedent cumulative rainfall is important for slope  
334 instability in models m77, m14, m771419 and m7714161921, while model m19 shows the lowest mean coefficient for this  
335 variable.

336 The intra event maximum rainfall intensity is also a relevant variable, but with a more complex influence. This variable is very  
337 important for model m14, with a strong destabilizing effect, but it is not included into model m19, and assumes a negative  
338 coefficient in m77.



		Coefficients					Frequencies				
G	Curvature	0.14	0.58	--	0.089	0.081	10	1	--	8	13
	Easternness	-0.15	0.62	-0.11	-0.073	--	48	50	30	3	--
	Max flow accumulation	0.3	--	0.25	0.25	0.25	50	--	50	50	50
	Mean flow accumulation	0.51	0.7	0.32	0.4	0.41	50	47	50	50	50
	Northernness	-0.49	-0.42	-0.32	-0.36	-0.35	50	1	50	50	50
	Planar curvature	--	--	0.1	--	--	--	--	1	--	--
	Profile curvature	--	--	--	-0.072	-0.084	--	--	--	3	7
	Slope	2.4	2.1	3.2	2.3	2.3	50	11	50	50	50
L	Basalts	--	--	--	--	--	--	--	--	--	--
	Calceschists	--	--	0.14	0.1	0.089	--	--	37	4	1
	Gabbros and peridotites	--	--	-0.4	--	--	--	--	9	--	--
	Gravels and sands	2	1.7	1.5	1.6	1.7	50	27	50	50	50
	Gypsum	--	--	0.11	0.088	0.11	--	--	5	1	15
	Limestones	--	--	--	--	--	--	--	--	--	--
	Marls	0.93	0.75	0.6	0.66	0.73	50	44	50	50	50
	Marls and sands	--	--	--	--	--	--	--	--	--	--
	Prasinities	--	--	0.12	--	0.088	--	--	22	--	1
	Sands and gravels	--	--	0.27	0.24	0.28	--	--	50	50	50
	Sandstone breccias	0.57	--	0.27	0.47	0.55	50	--	50	50	50
	Sandstones and conglomerates	--	--	0.32	0.16	0.21	--	--	41	42	50
	Sandstones and marls	0.29	0.44	0.17	0.21	0.24	50	39	45	50	50
	Sandstones and siltites	1.3	1.3	0.8	0.92	1	50	47	50	50	50
	Serpentinities	0.24	--	-0.36	--	--	1	--	6	--	--
Slates	--	--	--	--	--	--	--	--	--	--	
S	Clay content	0.62	0.85	0.5	0.53	0.51	50	3	49	50	50
	Coarse fragments	--	-1.2	-0.86	-0.24	-0.25	--	8	50	42	41
	Sand content	-0.85	--	-0.51	-0.55	-0.55	50	--	49	50	50
	Silt content	--	-0.6	0.37	--	0.22	--	1	50	--	1
U	Arable land	-0.25	-0.8	-0.18	-0.15	-0.21	29	3	1	6	1
	Areas with sparse/absent vegetation	-0.31	--	--	-0.16	-0.15	5	--	--	21	25
	Artificial non-agricultural green areas	--	--	--	--	--	--	--	--	--	--
	Heterogeneous agricultural areas	--	--	0.089	0.091	0.096	--	--	32	49	49
	Inland waters	-0.43	--	0.14	0.14	--	14	--	6	1	--
	Mining areas	--	--	--	--	--	--	--	--	--	--
	Permanent crops	-0.29	0.47	-0.11	-0.11	-0.099	49	1	29	37	38
	Permanent lawns	0.16	--	-0.16	--	--	10	--	30	--	--
	Road network	--	0.57	0.3	0.28	0.27	--	11	50	50	50
	Shrubby/herbaceous areas	0.21	0.7	--	0.21	0.21	50	50	--	50	50
Urbanized and productive areas	--	0.52	--	0.13	0.12	--	33	--	3	1	
Woods	0.27	0.63	--	0.17	0.17	13	1	--	38	46	
R	Antecedent cum rainfall (90 days)	0.93	1.8	0.21	1	1.7	50	43	37	50	50
	Intra event max rainfall intensity	-0.21	3.8	--	0.69	1.1	20	50	--	50	50

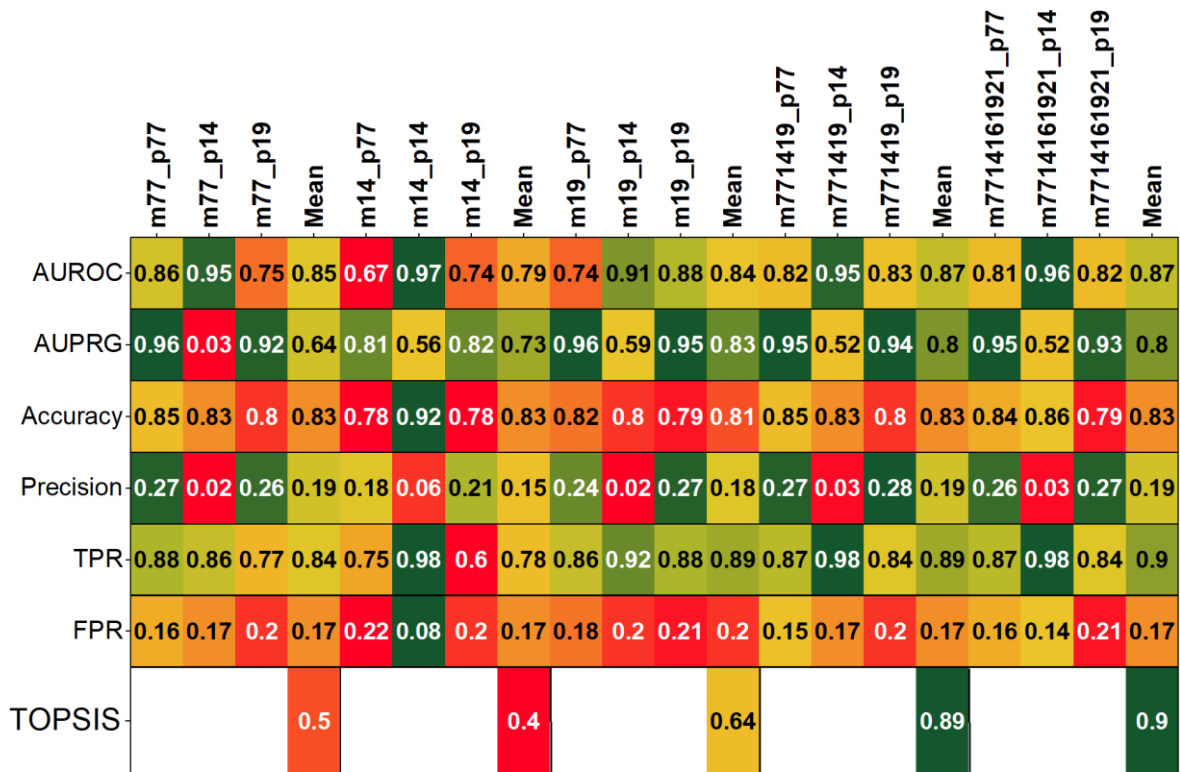
339

340 **Figure 6.** Variation of the median coefficient (left panel) and inclusion rate (frequency – right panel) of variable selection according  
 341 to the different training model, based on 50 iterations. Variables are aggregated in 5 groups (G = geomorphological parameters, L  
 342 = lithological parameters, S = soil grain size, U = land use and land cover parameters, R = rainfall parameters). Grey boxes indicate  
 343 that the variable was never chosen by the model.



344 Model m14 shows a good performance when evaluated over its validation dataset, with a mean AUROC value of 0.97 (highest  
 345 mean AUROC value among all the tested models), but it fails in predicting or hindcasting other landslide events, as indicated  
 346 by an interquartile range of AUROC values between 0.62 and 0.74 (Fig. S5), a low accuracy and a high FPR. Model m77  
 347 shows a high mean AUROC, but a low AUPRG, especially when trying to predict 2014 landslides, meaning that the model  
 348 output becomes less precise when ignoring the true negatives. On average, model m19 shows good prediction capabilities,  
 349 especially in terms of AUPRG. Models trained over multiple events show the best performance, and an associated reduction  
 350 in the variability of the final results. The mean AUROC value increases, as does the mean AUPRG. The inclusion of intense  
 351 rainfall events that did not lead to the triggering of slope instabilities results in small improvements in the general performance,  
 352 especially for the mean accuracy and FPR.

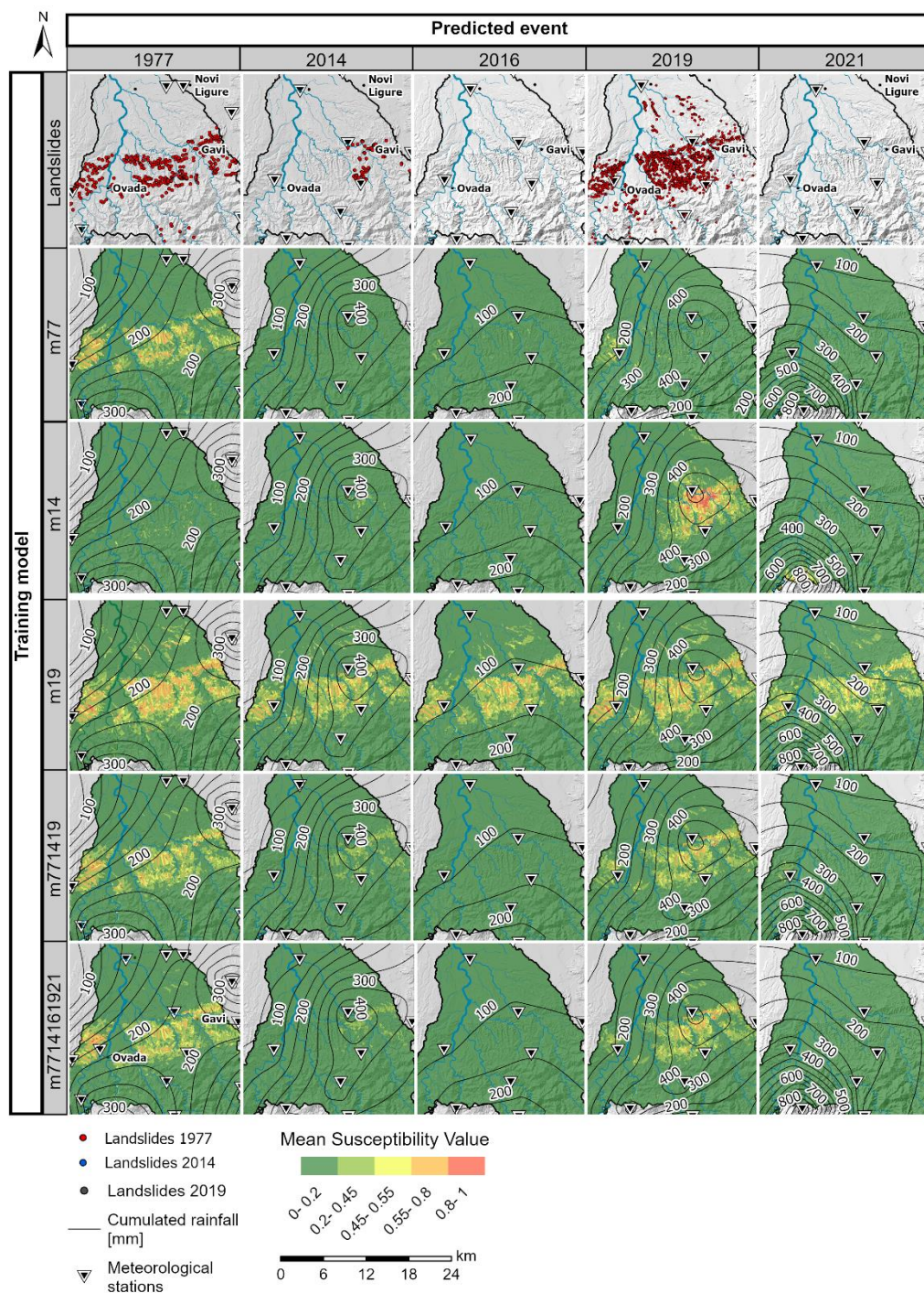
353 According to the TOPSIS classifier (Fig. 7), m7714161921 is the model with the highest relative closeness degree to the ideal  
 354 solution, obtained giving the same weight for the evaluation of all the scores (0.16 for all the metrics).



355  
 356 **Figure 7. AUROC, accuracy, precision, true positive rate TPR and false positive rate FPR obtained using the threshold that**  
 357 **minimizes the expected costs, calculated for each model assuming equal costs. For each model, the relative closeness degree of**  
 358 **alternatives to the ideal solution (Ci) and ranks of the evaluated models are also reported.**



359 **3.4 Model representation**



360

361 **Figure 8. Landslide susceptibility maps for the Orba basin. Columns refer to different training models, while rows refer to different**  
 362 **predicted or hindcasted events.**



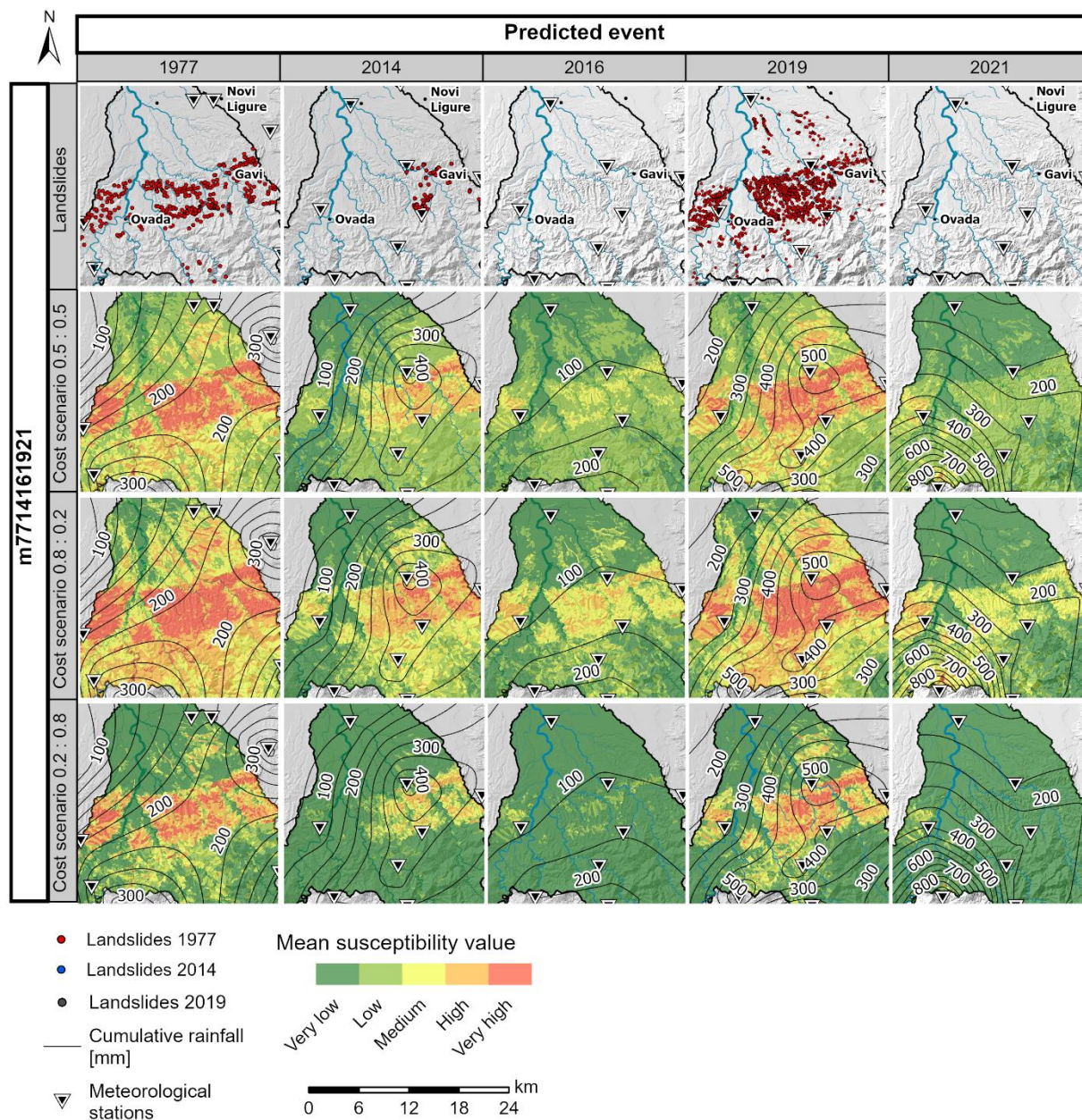


363 For each model, five rainfall events were used to produce the rainfall-based susceptibility maps (Fig. 8), obtaining different  
 364 maps for each model as a function of the event-specific rainfall values. From a simple visual inspection, comparing  
 365 susceptibility classes and landslide distribution, it is clear that models m14 and m19 are not able to correctly model landslide  
 366 susceptibility. As already seen in Fig. 6, the high coefficient of rainfall intensity in m14 makes susceptibility excessively  
 367 dependent on this variable, so that the resulting unstable units simply reflect its distribution. On the contrary, the exclusion of  
 368 rainfall intensity and the low coefficients of antecedent rainfall in m19 make the susceptibility maps almost constant for  
 369 different events. In addition, the model tends to overestimate unstable areas. Model m77 shows a better performance, but still  
 370 suffers from the low coefficient of maximum rainfall intensity, making also this model quite constant between different events,  
 371 thus predicting unstable areas also for the 2016 and 2021 events. Models m771419 and m7714161921 significantly outperform  
 372 the others, as they are able to classify the central part of the study area as unstable only for heavy rainfall events. However,  
 373 they tend to underestimate the percentage of unstable or very unstable slope units during the 1977, 2014 and 2019 events, with  
 374 less than 4% of the slope units classified as moderately, highly or very highly unstable. On the other hand, they correctly  
 375 classify all the slope units as stable when considering rainfall events that were not associated with landslides (p16 and p21).  
 376 Model m7714161921 also shows a slightly better ability to handle false positives when simulating non-triggering rainfall  
 377 events, as it can be seen in the last row of Fig. 6 for the prediction of m14, m16 and m21, especially in the western part of the  
 378 study area.

379 In general, the maps in Fig. 8 classified by using a rather standard partitioning of the susceptibility values into five classes (0  
 380 – 0.2, 0.2 – 0.45, 0.45 – 0.55, 0.55 – 0.8, 0.8 – 1) show an uneven distribution of slope units in the different classes, giving the  
 381 impression of either overestimation or underestimation. This problem was addressed with the new classification method based  
 382 on misclassification costs, which was applied to m7714161921 (ranked as the best performing model). For each of the three  
 383 considered scenarios the optimal cut-off threshold and the relative geometric progression were derived, considering different  
 384 misclassification cost ratios (Table 2). The class boundaries derived from the geometric progression were then used to  
 385 reclassify the susceptibility values, to produce optimised maps (Fig. 9). The optimal cut-off threshold decreases as the relative  
 386 cost of false negatives decreases, thus reducing the number of slope units classified as unstable.

387 **Table 2. Threshold values for m7714161921, for each of the proposed scenarios of relative costs. HST is the half-susceptibility**  
 388 **threshold corresponding to the value that minimizes the normalized expected cost for each cost scenario.**

Cost Scenarios	HST	VL	L	M	H	VH
$c(- +): c(+ -) = 0.5 : 0.5$	0.034	0.005	0.018	0.068	0.261	1.000
$c(- +): c(+ -) = 0.8 : 0.2$	0.010	0.018	0.068	0.261	1.000	0.005
$c(- +): c(+ -) = 0.2 : 0.8$	0.104	0.066	0.164	0.405	1.000	0.027



389

390 **Figure 9. Instability maps relative to the best performing model (m7714161921). Each row refers to a different relative cost scenario,**  
 391 **where the proportions refer to the ratio between costs associated to false negatives and false positives. Classes limits are defined**  
 392 **based on the optimal cut-off threshold and the relative geometric progression.**



## 393 4 Discussion

### 394 4.1 Landslide distribution analysis and prediction

395 This paper investigated the relationship between several spatially distributed variables (i.e., possible triggering factors) and  
396 the occurrence of shallow landslides through a logistic regression-based susceptibility analysis.

397 At a first visual inspection, the spatial distribution of the shallow landslides is fairly constant in all the available inventories,  
398 suggesting that shallow landslides in this area are modulated by rainfall, but controlled by other static parameters. In particular,  
399 landslides tend to occur in slope units with similar geomorphology and lithology (Fig. 4).

400 More specifically, beside the slope gradient, lithology appears to be the most important variable that controls landslide  
401 susceptibility (Fig. 6). Among all, the most prone lithologies in all the inventories are marls, sandstones and siltites, similarly  
402 to the results of Luino and Padano (1999) and Licata *et al.* (2023). The high importance given to gravels and sands, a lithology  
403 commonly found in alluvial flat areas, can be explained with the instability of fluvial terraces (Šilhán, 2022). Moreover, the  
404 lithology controls the grain size of the soil cover and, thus, the hydrological processes in the unsaturated zone. The sedimentary  
405 sequence in the central part of the area, overlaid by soils with a high clay content, is another important destabilizing factor in  
406 the model because of the poor draining capacity of clays. More interestingly, the southern metamorphic basement is commonly  
407 covered by soils rich in sand and coarse fragments, which have a strong stabilizing effect, probably correlated with a higher  
408 drainage capacity and friction angle.

409 Surprisingly, the role of land use does not appear to be relevant. In addition, the role of lithology may be strong enough to  
410 mask the land-use effect.

411 Looking at the variables related to rainfall dynamics, the cumulative antecedent rainfall is the most relevant in all regression  
412 models. In fact, it has been considered a proxy for the soil water content before the event, which for various authors it is pivotal  
413 for modelling shallow landslides (Bogaard and Greco, 2018; Marino *et al.*, 2020b). The intra event maximum rainfall intensity  
414 is also a relevant variable, but with a more complex influence. Being calculated with a 24 h aggregation time, this variable can  
415 be intended as a general descriptor of the entire rainfall event, representative of both the rainfall intensity and the daily  
416 cumulative value. Using a smaller aggregation time could help to differentiate the effects of these two descriptors, which was  
417 impossible for the event of 1977, as outlined in Sect. 4.2.

418 These parameters are also important to explain the spatial distribution of the landslide density. In particular, the analysis of the  
419 relationships between landslide density, the normalized maximum rainfall intensity over 24 hours and the normalized values  
420 of the antecedent cumulative rainfall suggest that landslide density appears to be controlled by the maximum rainfall intensity.  
421 This agrees with the mechanical explanation of shallow landslides triggering, controlled by soil saturation, leading to an  
422 increase in pore pressure and a loss of soil suction (Fredlund *et al.*, 1978). In addition, the antecedent condition shows a double  
423 role of setting a threshold required for landslide initiation (e.g. Crozier, 1999; Glade *et al.*, 2000; Godt *et al.*, 2006; Marino *et*  
424 *al.*, 2020b), and offsetting the relationship between landslide density and rainfall intensity.



425 Several basin-scale studies suggest that to quantify the shallow landslide susceptibility, the use of multitemporal inventories  
426 lead to better results (Reichenbach et al., 2018), while others affirm that this is not always associated with a model performance  
427 improvement (Ozturk et al., 2021; Smith et al., 2021). Results show that, for the Orba basin, models trained over a single  
428 landslide event are not capable of catching the real processes underlying the instability phenomena, despite the high landslide  
429 density and the good performance when using the test dataset. Thus, they are unable to predict landslide events associated with  
430 different rainfall characteristics. In particular, m14, being the smaller landslide inventory and more limited in the extend of the  
431 affected area, shows the best performance when tested against itself (Fig. 7 and Fig. S5), and the worst performance when used  
432 to model other events, producing maps with an exaggerated landslide susceptibility in areas with high precipitation. The  
433 inclusion of multiple events helps in stabilising the effect exerted by the different controlling variables, thus providing more  
434 reliable prediction/hindcast susceptibility maps.

435 The evaluation of the performance of regression models is always challenging, especially when using an input dataset with a  
436 skewed distribution (e.g. Provost *et al.*, 1998; Davis and Goadrich, 2006; Drummond and Holte, 2006). AUROC, which is the  
437 most used evaluation method in the literature (Reichenbach et al., 2018) suffers from an overly optimistic evaluation while  
438 misclassifying the samples that belongs to the underrepresented class. This is the case of model m77 when predicting 2014  
439 event. On the other side, AUPRG shows high values when model m77 predicts 2019 event, even if large parts of the area  
440 affected by landslides is predicted as stable. The other indices are cut-off dependent, and they do not show any capabilities to  
441 discriminate among the different models. For these reasons, the multi-criteria TOPSIS model was used to consider the  
442 contribution of all the indices. Interestingly, the TOPSIS classification shows significant variations across the models where  
443 single appear to show no significance. Based on the TOPSIS evaluation, the multitemporal models outperform the single event  
444 models, confirming what discussed above. In particular, the model with the highest prediction capabilities is m7714161921,  
445 suggesting that the inclusion of non-triggering rainfall events helps in defining the rainfall threshold to trigger instabilities in  
446 different parts of the study area.

447 For the representation of the results, the classification scheme typically adopted in the literature does not account for  
448 misclassification costs (Cantarino et al., 2019), which are implicitly assumed equal. However, since the misclassifications  
449 costs are often not equal, the total misclassification cost can be reduced by playing on the degree of conservativeness of the  
450 models in order to reduce the false negatives or false positives rates, thus increasing or decreasing what is classified as unstable.  
451 This required a new classification scheme to adjust the thresholds used for susceptibility classification according to the selected  
452 proportion of misclassification costs.

453 Scenario 2, where the costs of false negatives are higher, is the most conservative because the classification is forced towards  
454 instability to keep the false negatives rate low. On the contrary, scenario 3, where the costs of false positives are higher, shows  
455 the highest percentage of stable slope units. Scenario 1 considers equal costs for false positives and false negatives, and  
456 produces intermediate results. The strong differences between these scenarios suggest that the use of cost curves for the  
457 landslide susceptibility model could be a valuable tool in the final stages of a susceptibility analysis, when slope units need to  
458 be classified. This approach allows for different classification thresholds based on cost combinations, enabling the evaluation



459 of their consequences. Costs may include direct costs like damage to infrastructure and loss of life, and indirect costs like  
460 traffic disruptions and lost productivity (Sala et al., 2021). While this work uses different cost ratio scenarios to demonstrate  
461 the approach's potential, more detailed analyses could provide precise cost quantifications, considering that costs may vary  
462 across different parts of the study area.

#### 463 **4.2 Challenges, uncertainties, and limitations**

464 It is necessary to underline possible uncertainties and assumptions regarding the input datasets and the modelling strategies,  
465 so that the limitations of our findings are made clear. Two main limitations can potentially affect the results of these analyses:  
466 the consideration of land use and land cover as a static variable and the use of an old landslide inventory.

467 First, land use and land cover can vary greatly over time. Considering this variable as static is mainly due to a lack of  
468 information, since the only other dataset provided by ARPA Piemonte dates to 2010, and the analysis of satellite images,  
469 besides being beyond the purpose of this study, was not possible for the 1977 event. An analysis of the land use change between  
470 two available datasets (2010 and 2021) within the Orba basin revealed that permanent crops decreased by 6% and meadows  
471 by almost 2%, while the areas characterised by shrub and herbaceous vegetation increased by 4% and the woods by almost  
472 4%. However, these changes can be considered negligible in the analyses, given the very low influence of the land use variables  
473 in the logistic regression. This is in contrast with the conclusions of many other studies (for example Bernardie *et al.*, 2017;  
474 Persichillo *et al.*, 2017; Hürlimann *et al.*, 2022), suggesting that this relationship could be further analysed in future studies.

475 The second limitation is posed by the inclusion of an older event (1977) with higher uncertainty of both rainfall pattern and  
476 landslide distribution. Data from the ARPA Piemonte and ARPA Liguria weather stations were used to analyse the rainfall  
477 pattern. However, only 36 stations were active in 1977, 26% less than in 2014 and 2019, and most of them are located outside  
478 the region of interest (Fig. 2). This uncertainty in the rainfall pattern could affect the modelling, especially in the central part  
479 of the basin. In addition, data for 1977 were only available with a daily time step, making it impossible to use multiple different  
480 aggregation times. The landslide inventory of the 1977 event represents landslides as areas affected by diffuse shallow  
481 landslides rather than individual polygons. This affects the landslide distribution and density analysis. However, the choice to  
482 use slope units for analysis mitigated this difference in the inventories. Finally, as mentioned above, the use of this landslide  
483 event precluded the use of satellite products; therefore, some factors that could improve susceptibility analyses, such as  
484 satellite-based antecedent soil moisture, could not be incorporated into the model.

#### 485 **5 Conclusions**

486 This study demonstrates the feasibility of using logistic regression to model the effects of extreme rainfall events on the stability  
487 of a complex study area, such as the Orba basin in the Piedmont region of Italy. In this area, the spatial distribution of shallow  
488 landslides reflects the distribution of lithology and geomorphology, thus showing a similar pattern for different rainfall  
489 scenarios.



490 In such conditions, the development of a rainfall dependent model capable of simulating different susceptibility scenarios is  
491 more challenging, and requires a careful calibration of the model with representative and significant rainfall events over a  
492 multi-temporal dataset. In fact, the use of single events may be problematic. For example, a rainfall event that is spatially  
493 concentrated in a small area with specific geological characteristics (such as in 2019 for the study area) could overestimate the  
494 role of such characteristics despite the rainfall, producing biased scenarios. On the contrary, a model trained on an extreme  
495 localised event spanning different geological conditions (such as the 2014 event) may overestimate the role of rainfall at the  
496 expense of geology. Finally, a rainfall event evenly distributed over the area (such as in 1977) would produce a model that  
497 underestimates the role of rainfall in controlling the landslide pattern.

498 To avoid such effects, an ensemble of rainfall events is preferable to better unravel the effects of the triggering variables, and  
499 also to compensate for local misleading effects that may arise from the use of a single rainfall event. The use of rainfall events  
500 that did not trigger landslides may also be helpful for such compensation. The proposed strategy for selecting the best ensemble  
501 of rainfall events was based on the maximization of the AUROC, AUPRG, accuracy and precision, and the minimization of  
502 the expected misclassification costs.

503 Eventually, misclassification costs were adopted as a criterion to define the susceptibility classes for the practical use of the  
504 resulting maps; this highlights the need to give importance to the classification process, which should be tailored to the needs  
505 of the end users and on the purpose of the final products.

#### 506 **Data availability**

507 Data for Regione Piemonte are publicly accessible at <https://geoportale.igr.piemonte.it/cms/> (Geoportale Regione Piemonte)  
508 and at <https://www.arpa.piemonte.it/> (ARPA Piemonte).

#### 509 **Supplement link**

510 The supplement related to this article is available online.

#### 511 **Author contribution**

512 MF: conceptualization, data preparation, analysis/coding, writing – original draft. AP: conceptualization, visualization, writing  
513 – review and editing. PF: conceptualization, validation, writing – original draft. GC: conceptualization, writing – review and  
514 editing.

#### 515 **Competing interests**

516 The authors declare that they have no conflict of interest.



517 **Disclaimer**

518 Publisher's note: Copernicus Publications remains neutral with regard to jurisdictional claims in published maps and  
519 institutional affiliations.

520 **Acknowledgements**

521 The authors would like to thank Luca Lanteri and the Operative Group "Landslides monitoring and geological studies" of the  
522 Regional Environmental Protection Agency of Piedmont for the sharing of landslide mapping data related to the 2019 landslide  
523 event.



## 524 References

- 525 Alvioli, M., Marchesini, I., Reichenbach, P., Rossi, M., Ardizzone, F., Fiorucci, F., and Guzzetti, F.: Automatic delineation of  
526 geomorphological slope units with r.slopeunits v1.0 and their optimization for landslide susceptibility modeling, *Geosci.*  
527 *Model Dev.*, 9, 3975–3991, <https://doi.org/10.5194/gmd-9-3975-2016>, 2016.
- 528 ARPA Piemonte: Eventi idrometeorologici dal 19 al 24 Ottobre 2019 - Parte I, 2019.
- 529 Bandis, S. C., Delmonaco, G., and Dutto, F.: Landslide phenomena during the extreme meteorological event of 4-6- November  
530 1994 in Piemonte Region in N. Italy, *Int. Symp. Landslide*, 1996.
- 531 Baum, R. L., Savage, W. Z., and Godt, J. W.: TRIGRS — A Fortran Program for Transient Rainfall Infiltration and Grid-  
532 Based Regional Slope-Stability Analysis, Version 2.0, U.S. Geol. Surv. Open-File Rep., 75, 2008.
- 533 Beguería, S.: Validation and Evaluation of Predictive Models in Hazard Assessment and Risk Management, *Nat. Hazards*, 37,  
534 315–329, <https://doi.org/10.1007/s11069-005-5182-6>, 2006.
- 535 Bernardie, S., Vandromme, R., Mariotti, A., Houet, T., Grémont, M., Grandjean, G., Bouroullec, I., and Thiery, Y.: Estimation  
536 of Landslides Activities Evolution Due to Land–Use and Climate Change in a Pyrenean Valley, in: *Advancing Culture of*  
537 *Living with Landslides*, Springer International Publishing, Cham, 859–867, [https://doi.org/10.1007/978-3-319-53498-5\\_98](https://doi.org/10.1007/978-3-319-53498-5_98),  
538 2017.
- 539 Bogaard, T. and Greco, R.: Invited perspectives: Hydrological perspectives on precipitation intensity-duration thresholds for  
540 landslide initiation: Proposing hydro-meteorological thresholds, *Nat. Hazards Earth Syst. Sci.*, 18, 31–39,  
541 <https://doi.org/10.5194/nhess-18-31-2018>, 2018.
- 542 Bordoni, M., Vivaldi, V., Lucchelli, L., Ciabatta, L., Brocca, L., Galve, J. P., and Meisina, C.: Development of a data-driven  
543 model for spatial and temporal shallow landslide probability of occurrence at catchment scale, *Landslides*, 18, 1209–1229,  
544 <https://doi.org/10.1007/s10346-020-01592-3>, 2021.
- 545 Brenning, A.: Spatial prediction models for landslide hazards: review, comparison and evaluation, *Nat. Hazards Earth Syst.*  
546 *Sci.*, 5, 853–862, <https://doi.org/10.5194/nhess-5-853-2005>, 2005.
- 547 Caine, N.: The Rainfall Intensity: Duration Control of Shallow Landslides and Debris Flows, *Geogr. Ann. Ser. A, Phys. Geogr.*,  
548 62, 23–27, 1980.
- 549 Camera, C. A. S., Bajni, G., Corno, I., Raffa, M., Stevenazzi, S., and Apuani, T.: Introducing intense rainfall and snowmelt  
550 variables to implement a process-related non-stationary shallow landslide susceptibility analysis, *Sci. Total Environ.*, 786,  
551 147360, <https://doi.org/10.1016/j.scitotenv.2021.147360>, 2021.
- 552 Campbell, R. H.: Soil Slips, Debris Flows, and Rainstorms in the Santa Monica Mountains and Vicinity, Southern California,  
553 U.S. Geol. Surv. Prof. Pap. 851, 51 pages, 1975.
- 554 Cantarino, I., Carrion, M. A., Goerlich, F., and Martinez Ibañez, V.: A ROC analysis-based classification method for landslide  
555 susceptibility maps, *Landslides*, 16, 265–282, <https://doi.org/10.1007/s10346-018-1063-4>, 2019.
- 556 Carrara, A.: Multivariate models for landslide hazard evaluation, *J. Int. Assoc. Math. Geol.*, 15, 403–426,





- 557 <https://doi.org/10.1007/BF01031290>, 1983.
- 558 Carrara, A., Cardinali, M., Detti, R., Guzzetti, F., Pasqui, V., and Reichenbach, P.: GIS techniques and statistical models in  
559 evaluating landslide hazard, *Earth Surf. Process. Landforms*, 16, 427–445, <https://doi.org/10.1002/esp.3290160505>, 1991.
- 560 Carrara, A., Crosta, G., and Frattini, P.: Comparing models of debris-flow susceptibility in the alpine environment,  
561 *Geomorphology*, 94, 353–378, <https://doi.org/10.1016/j.geomorph.2006.10.033>, 2008.
- 562 Coletti, G., Basso, D., Frixa, A., and Corselli, C.: Transported Rhodoliths Witness the lost carbonate factory: A case history  
563 from the miocene pietra da cantoni limestone (Nw Italy), *Riv. Ital. di Paleontol. e Stratigr.*, 121, 345–368,  
564 <https://doi.org/10.13130/2039-4942/6522>, 2015.
- 565 ERA5-Land hourly data from 1950 to present.:
- 566 Crosta, G.: Regionalization of rainfall thresholds: An aid to landslide hazard evaluation, *Environ. Geol.*, 35, 131–145,  
567 <https://doi.org/10.1007/s002540050300>, 1998.
- 568 Crosta, G. B. and Frattini, P.: Distributed modelling of shallow landslides triggered by intense rainfall, *Nat. Hazards Earth*  
569 *Syst. Sci.*, 3, 81–93, <https://doi.org/10.5194/nhess-3-81-2003>, 2003.
- 570 Crozier, M. J.: Prediction of rainfall-triggered landslides: A test of the antecedent water status model, *Earth Surf. Process.*  
571 *Landforms*, 24, 825–833, 1999.
- 572 Cruden, D. M. and Varnes, D. J.: Chapter 3 Landslide Types and Processes, *Landslides Investig. Mitigation, Transp. Res.*  
573 *Board Spec. Rep. 247*, Washingt. D.C., 36–75, 1996.
- 574 Davis, J. and Goadrich, M.: The Relationship Between Precision-Recall and ROC Curves, *Proc. 23rd Int. Conf. Mach. Learn.*  
575 *Pittsburgh, PA*, <https://doi.org/10.1109/ICACCCN51052.2020.9362793>, 2006.
- 576 Drummond, C. and Holte, R. C.: Cost curves: An improved method for visualizing classifier performance, *Mach. Learn.*, 65,  
577 95–130, <https://doi.org/10.1007/s10994-006-8199-5>, 2006.
- 578 Van Den Eeckhaut, M., Poesen, J., Govers, G., Verstraeten, G., and Demoulin, A.: Characteristics of the size distribution of  
579 recent and historical landslides in a populated hilly region, *Earth Planet. Sci. Lett.*, 256, 588–603,  
580 <https://doi.org/10.1016/j.epsl.2007.01.040>, 2007.
- 581 Fioravanti, G., Frascchetti, P., Lena, F., Perconti, W., and Emanuela, P. (ISPRA): I normali climatici 1991-2020 di temperatura  
582 e precipitazione in Italia, *Stato dell’ambiente*, 9, 2022.
- 583 Flach, P. A. and Kull, M.: Precision-Recall-Gain curves: PR analysis done right, *Adv. Neural Inf. Process. Syst.*, 2015-Janua,  
584 838–846, 2015.
- 585 Frattini, P. and Crosta, G. B.: The role of material properties and landscape morphology on landslide size distributions, *Earth*  
586 *Planet. Sci. Lett.*, 361, 310–319, <https://doi.org/10.1016/j.epsl.2012.10.029>, 2013.
- 587 Frattini, P., Crosta, G., and Sosio, R.: Approaches for defining thresholds and return periods for rainfall-triggered shallow  
588 landslides, *Hydrol. Process.*, 23, 1444–1460, <https://doi.org/10.1002/hyp.7269>, 2009.
- 589 Frattini, P., Crosta, G., and Carrara, A.: Techniques for evaluating the performance of landslide susceptibility models, *Eng.*  
590 *Geol.*, 111, 62–72, <https://doi.org/10.1016/j.enggeo.2009.12.004>, 2010.



- 591 Fredlund, D. G., Morgenstern, N. R., and Widger, R. A.: Shear Strength of Unsaturated Soils, *Can. Geotech. J.*, 15, 313–321,  
592 <https://doi.org/10.1139/t78-029>, 1978.
- 593 Gilbert, G. K.: Finley’s Tornado Predictions, *Am. Meteorol. J.*, 1, 166–172, 1884.
- 594 Glade, T., Crozier, M., and Smith, P.: Applying probability determination to refine landslide-triggering rainfall thresholds  
595 using an empirical “Antecedent Daily Rainfall Model,” *Pure Appl. Geophys.*, 157, 1059–1079,  
596 <https://doi.org/10.1007/s000240050017>, 2000.
- 597 Godt, J. W., Baum, R. L., and Chleborad, A. F.: Rainfall characteristics for shallow landsliding in Seattle, Washington, USA,  
598 *Earth Surf. Process. Landforms*, 31, 97–110, <https://doi.org/10.1002/esp.1237>, 2006.
- 599 Goetz, J. N., Brenning, A., Petschko, H., and Leopold, P.: Evaluating machine learning and statistical prediction techniques  
600 for landslide susceptibility modeling, *Comput. Geosci.*, 81, 1–11, <https://doi.org/10.1016/j.cageo.2015.04.007>, 2015.
- 601 Guzzetti, F., Carrara, A., Cardinali, M., and Reichenbach, P.: Landslide hazard evaluation: a review of current techniques and  
602 their application in a multi-scale study, Central Italy, *Geomorphology*, 13, 1995, 1999.
- 603 Guzzetti, F., Peruccacci, S., Rossi, M., and Stark, C. P.: Rainfall thresholds for the initiation of landslides in central and  
604 southern Europe, *Meteorol. Atmos. Phys.*, 98, 239–267, <https://doi.org/10.1007/s00703-007-0262-7>, 2007.
- 605 Hanley, J. A. and McNeil, B. J.: The meaning and use of the area under a receiver operating characteristic (ROC) curve,  
606 *Radiology*, 143, 29–36, <https://doi.org/10.1148/radiology.143.1.7063747>, 1982.
- 607 Heidke, P.: Berechnung Des Erfolges Und Der Güte Der Windstärkevorhersagen Im Sturmwarnungsdienst, *Geogr. Ann.*, 8,  
608 301–349, <https://doi.org/10.1080/20014422.1926.11881138>, 1926.
- 609 Hersbach, H., Bell, B., Berrisford, P., Hirahara, S., Horányi, A., Muñoz-Sabater, J., Nicolas, J., Peubey, C., Radu, R., Schepers,  
610 D., Simmons, A., Soci, C., Abdalla, S., Abellan, X., Balsamo, G., Bechtold, P., Biavati, G., Bidlot, J., Bonavita, M., De Chiara,  
611 G., Dahlgren, P., Dee, D., Diamantakis, M., Dragani, R., Flemming, J., Forbes, R., Fuentes, M., Geer, A., Haimberger, L.,  
612 Healy, S., Hogan, R. J., Hólm, E., Janisková, M., Keeley, S., Laloyaux, P., Lopez, P., Lupu, C., Radnoti, G., de Rosnay, P.,  
613 Rozum, I., Vamborg, F., Villaume, S., and Thépaut, J. N.: The ERA5 global reanalysis, *Q. J. R. Meteorol. Soc.*, 146, 1999–  
614 2049, <https://doi.org/10.1002/qj.3803>, 2020.
- 615 Hosmer, D. W. and Lemeshow, S.: *Applied Logistic Regression*, John Wiley & Sons, Inc., Hoboken, NJ, USA,  
616 <https://doi.org/10.1002/0471722146>, 2000.
- 617 Huang, F., Cao, Z., Guo, J., Jiang, S. H., Li, S., and Guo, Z.: Comparisons of heuristic, general statistical and machine learning  
618 models for landslide susceptibility prediction and mapping, *Catena*, 191, 104580,  
619 <https://doi.org/10.1016/j.catena.2020.104580>, 2020.
- 620 Hungr, O.: A review of landslide hazard and risk assessment methodology, *Landslides Eng. Slopes. Exp. Theory Pract.*, 1, 3–  
621 27, <https://doi.org/10.1201/b21520-3>, 2016.
- 622 Hürlimann, M., Guo, Z., Puig-Polo, C., and Medina, V.: Impacts of future climate and land cover changes on landslide  
623 susceptibility: regional scale modelling in the Val d’Aran region (Pyrenees, Spain), *Landslides*, 19, 99–118,  
624 <https://doi.org/10.1007/s10346-021-01775-6>, 2022.



- 625 Hwang, C.-L. and Yoon, K.: Multiple Attribute Decision Making: methods and applications a state-of-the-art survey, Springer  
626 Sci. Bus. Media, 186, 2012.
- 627 INTERREG IIC: Descrizione dei principali eventi alluvionali che hanno interessato la regione Piemonte, Liguria e nella  
628 Spagna Nord Orientale, 90–94 pp., 1998.
- 629 ISPRA: Dissesto idrogeologico in Italia: pericolosità e indicatori di rischio, 183 pp., 2021.
- 630 Iverson, R. M.: Landslide triggering by rain infiltration, *Water Resour. Res.*, 36, 1897–1910,  
631 <https://doi.org/10.1029/2000WR900090>, 2000.
- 632 Jacobs, L., Kervyn, M., Reichenbach, P., Rossi, M., Marchesini, I., Alvioli, M., and Dewitte, O.: Regional susceptibility  
633 assessments with heterogeneous landslide information: Slope unit- vs. pixel-based approach, *Geomorphology*, 356, 107084,  
634 <https://doi.org/10.1016/j.geomorph.2020.107084>, 2020.
- 635 Jenks, G. F.: The data model concept in statistical mapping., *Int. Yearb. Cartogr.*, 7, 186–190, 1967.
- 636 Jones, J. N., Boulton, S. J., Bennett, G. L., Stokes, M., and Whitworth, M. R. Z.: Temporal Variations in Landslide  
637 Distributions Following Extreme Events: Implications for Landslide Susceptibility Modeling, *J. Geophys. Res. Earth Surf.*,  
638 126, 1–26, <https://doi.org/10.1029/2021JF006067>, 2021.
- 639 Kirschbaum, D. and Stanley, T.: Satellite-Based Assessment of Rainfall-Triggered Landslide Hazard for Situational  
640 Awareness, *Earth's Futur.*, 6, 505–523, <https://doi.org/10.1002/2017EF000715>, 2018.
- 641 Knevels, R., Petschko, H., Proske, H., Leopold, P., Maraun, D., and Brenning, A.: Event-based landslide modeling in the  
642 styrian basin, Austria: Accounting for time-varying rainfall and land cover, *Geosci.*, 10, 1–27,  
643 <https://doi.org/10.3390/geosciences10060217>, 2020.
- 644 Licata, M., Buleo Tebar, V., Seitone, F., and Fubelli, G.: The Open Landslide Project (OLP), a New Inventory of Shallow  
645 Landslides for Susceptibility Models: The Autumn 2019 Extreme Rainfall Event in the Langhe-Monferrato Region  
646 (Northwestern Italy), *Geosci.*, 13, <https://doi.org/10.3390/geosciences13100289>, 2023.
- 647 Lombardo, L. and Mai, P. M.: Presenting logistic regression-based landslide susceptibility results, *Eng. Geol.*, 244, 14–24,  
648 <https://doi.org/10.1016/j.enggeo.2018.07.019>, 2018.
- 649 Lombardo, L., Opitz, T., Ardizzone, F., Guzzetti, F., and Huser, R.: Space-time landslide predictive modelling, *Earth-Science*  
650 *Rev.*, 209, 103318, <https://doi.org/10.1016/j.earscirev.2020.103318>, 2020.
- 651 Lu, N. and Godt, J.: Infinite slope stability under steady unsaturated seepage conditions, *Water Resour. Res.*, 44, 1–13,  
652 <https://doi.org/10.1029/2008WR006976>, 2008.
- 653 Luino, F.: Sequence of instability processes triggered by heavy rainfall in the Northern Italy, *Geomorphology*, 66, 13–39,  
654 <https://doi.org/10.1016/j.geomorph.2004.09.010>, 2005.
- 655 Luino, F. and Padano, B.: The Flood and Landslide Event of November 4-6 1994 in Piedmont Region ( Northwestern Italy ):  
656 Causes and Related Effects in Tanaro, 24, 123–129, 1999.
- 657 Malamud, B. D., Turcotte, D. L., Guzzetti, F., and Reichenbach, P.: Landslide inventories and their statistical properties, *Earth*  
658 *Surf. Process. Landforms*, 29, 687–711, <https://doi.org/10.1002/esp.1064>, 2004.



- 659 Mandarino, A., Luino, F., and Faccini, F.: Flood-induced ground effects and flood-water dynamics for hydro-geomorphic  
660 hazard assessment: the 21–22 October 2019 extreme flood along the lower Orba River (Alessandria, NW Italy), *J. Maps*, 17,  
661 136–151, <https://doi.org/10.1080/17445647.2020.1866702>, 2021.
- 662 Maraun, D., Knevels, R., Mishra, A. N., Truhetz, H., Bevacqua, E., Proske, H., Zappa, G., Brenning, A., Petschko, H., Schaffer,  
663 A., Leopold, P., and Puxley, B. L.: A severe landslide event in the Alpine foreland under possible future climate and land-use  
664 changes, *Commun. Earth Environ.*, 3, 1–11, <https://doi.org/10.1038/s43247-022-00408-7>, 2022.
- 665 Marc, O., Gosset, M., Saito, H., Uchida, T., and Malet, J. P.: Spatial Patterns of Storm-Induced Landslides and Their Relation  
666 to Rainfall Anomaly Maps, *Geophys. Res. Lett.*, 46, 11167–11177, <https://doi.org/10.1029/2019GL083173>, 2019.
- 667 Marino, P., Peres, D. J., Cancelliere, A., Greco, R., and Bogaard, T. A.: Soil moisture information can improve shallow  
668 landslide forecasting using the hydrometeorological threshold approach, *Landslides*, 17, 2041–2054,  
669 <https://doi.org/10.1007/s10346-020-01420-8>, 2020a.
- 670 Marino, P., Peres, D. J., Cancelliere, A., Greco, R., and Bogaard, T. A.: Soil moisture information can improve shallow  
671 landslide forecasting using the hydrometeorological threshold approach, *Landslides*, 17, 2041–2054,  
672 <https://doi.org/10.1007/s10346-020-01420-8>, 2020b.
- 673 Mason, P. J. and Rosenbaum, M. S.: Geohazard mapping for predicting landslides: An example from the Langhe Hills in  
674 Piemonte, NW Italy, *Q. J. Eng. Geol. Hydrogeol.*, 35, 317–326, <https://doi.org/10.1144/1470-9236/00047>, 2002.
- 675 Montgomery, D. R. and Dietrich, W. E.: A physically based model for the topographic control on shallow landsliding, *Water*  
676 *Resour. Res.*, 30, 1153–1171, <https://doi.org/10.1029/93WR02979>, 1994.
- 677 Montrasio, L., Schilirò, L., and Terrone, A.: Physical and numerical modelling of shallow landslides, *Landslides*, 13, 873–  
678 883, <https://doi.org/10.1007/s10346-015-0642-x>, 2016.
- 679 Moreno, M., Lombardo, L., Crespi, A., Zellner, P. J., Mair, V., Pittore, M., van Westen, C., and Steger, S.: Space-time data-  
680 driven modeling of precipitation-induced shallow landslides in South Tyrol, Italy, *Sci. Total Environ.*, 912, 169166,  
681 <https://doi.org/10.1016/j.scitotenv.2023.169166>, 2024.
- 682 Muñoz-Sabater, J., Dutra, E., Agustí-Panareda, A., Albergel, C., Arduini, G., Balsamo, G., Boussetta, S., Choulga, M.,  
683 Harrigan, S., Hersbach, H., Martens, B., Miralles, D. G., Piles, M., Rodríguez-Fernández, N. J., Zsoter, E., Buontempo, C.,  
684 and Thépaut, J. N.: ERA5-Land: A state-of-the-art global reanalysis dataset for land applications, *Earth Syst. Sci. Data*, 13,  
685 4349–4383, <https://doi.org/10.5194/essd-13-4349-2021>, 2021.
- 686 Nam, K., Kim, J., and Chae, B.: Exploring class imbalance with under-sampling, over-sampling, and hybrid sampling based  
687 on Mahalanobis distance for landslide susceptibility assessment: a case study of the 2018 Iburi earthquake induced landslides  
688 in Hokkaido, Japan, *Geosci. J.*, 28, 71–94, <https://doi.org/10.1007/s12303-023-0033-6>, 2024.
- 689 Ozturk, U., Pittore, M., Behling, R., Roessner, S., Andreani, L., and Korup, O.: How robust are landslide susceptibility  
690 estimates?, *Landslides*, 18, 681–695, <https://doi.org/10.1007/s10346-020-01485-5>, 2021.
- 691 Peirce, C. S.: The numerical measure of the success of predictions, *Science*, 453–454, 1884.
- 692 Persichillo, M. G., Bordoni, M., and Meisina, C.: The role of land use changes in the distribution of shallow landslides, *Sci.*



- 693 Total Environ., 574, 924–937, <https://doi.org/10.1016/j.scitotenv.2016.09.125>, 2017.
- 694 Petley, D.: Global patterns of loss of life from landslides, *Geology*, 40, 927–930, <https://doi.org/10.1130/G33217.1>, 2012.
- 695 Piana, F., Fioraso, G., Irace, A., Mosca, P., D’Atri, A., Barale, L., Falletti, P., Monegato, G., Morelli, M., Tallone, S., and  
696 Vigna, G. B.: Geology of Piemonte region (NW Italy, Alps–Apennines interference zone), *J. Maps*, 13, 395–405,  
697 <https://doi.org/10.1080/17445647.2017.1316218>, 2017.
- 698 Poggio, L., De Sousa, L. M., Batjes, N. H., Heuvelink, G. B. M., Kempen, B., Ribeiro, E., and Rossiter, D.: SoilGrids 2.0:  
699 Producing soil information for the globe with quantified spatial uncertainty, *Soil*, 7, 217–240, [https://doi.org/10.5194/soil-7-](https://doi.org/10.5194/soil-7-217-2021)  
700 217-2021, 2021.
- 701 Provost, F. and Fawcett, T.: Robust classification for imprecise environments, *Mach. Learn.*, 42, 203–231,  
702 <https://doi.org/10.1023/A:1007601015854>, 2001.
- 703 Provost, F., Fawcett, T., and Kohavi, R.: The case against accuracy estimation for comparing induction algorithms, *Int. Conf.*  
704 *Mach. Learn.*, 445, 1998.
- 705 Raghavan, V., Bollmann, P., and Jung, G. S.: A Critical Investigation of Recall and Precision as Measures of Retrieval System  
706 Performance, *ACM Trans. Inf. Syst.*, 7, 205–229, <https://doi.org/10.1145/65943.65945>, 1989.
- 707 Reichenbach, P., Rossi, M., Malamud, B. D., Mihir, M., and Guzzetti, F.: A review of statistically-based landslide  
708 susceptibility models, *Earth-Science Rev.*, 180, 60–91, <https://doi.org/10.1016/j.earscirev.2018.03.001>, 2018.
- 709 Saito, T. and Rehmsmeier, M.: The precision-recall plot is more informative than the ROC plot when evaluating binary  
710 classifiers on imbalanced datasets, *PLoS One*, 10, 1–21, <https://doi.org/10.1371/journal.pone.0118432>, 2015.
- 711 Sala, G., Lanfranconi, C., Frattini, P., Rusconi, G., and Crosta, G. B.: Cost-sensitive rainfall thresholds for shallow landslides,  
712 *Landslides*, 18, 2979–2992, <https://doi.org/10.1007/s10346-021-01707-4>, 2021.
- 713 Samia, J., Temme, A., Bregt, A. K., Wallinga, J., Stuiver, J., Guzzetti, F., Ardizzone, F., and Rossi, M.: Implementing landslide  
714 path dependency in landslide susceptibility modelling, *Landslides*, 15, 2129–2144, [https://doi.org/10.1007/s10346-018-1024-](https://doi.org/10.1007/s10346-018-1024-y)  
715 y, 2018.
- 716 Segoni, S., Tofani, V., Rosi, A., Catani, F., and Casagli, N.: Combination of rainfall thresholds and susceptibility maps for  
717 dynamic landslide hazard assessment at regional scale, *Front. Earth Sci.*, 6, <https://doi.org/10.3389/feart.2018.00085>, 2018.
- 718 Šilhán, K.: Dendrogeomorphological analysis of landslides on the undercut river terrace bank (a case study in Czech Republic),  
719 *Landslides*, 19, 621–635, <https://doi.org/10.1007/s10346-021-01833-z>, 2022.
- 720 Smith, H. G., Spiekermann, R., Betts, H., and Neverman, A. J.: Comparing methods of landslide data acquisition and  
721 susceptibility modelling: Examples from New Zealand, *Geomorphology*, 381, 107660,  
722 <https://doi.org/10.1016/j.geomorph.2021.107660>, 2021.
- 723 Smith, H. G., Neverman, A. J., Betts, H., and Spiekermann, R.: The influence of spatial patterns in rainfall on shallow  
724 landslides, *Geomorphology*, 437, 108795, <https://doi.org/10.1016/j.geomorph.2023.108795>, 2023.
- 725 Steger, S., Brenning, A., Bell, R., and Glade, T.: The propagation of inventory-based positional errors into statistical landslide  
726 susceptibility models, *Nat. Hazards Earth Syst. Sci.*, 16, 2729–2745, <https://doi.org/10.5194/nhess-16-2729-2016>, 2016.



- 727 Thomas, M. A., Mirus, B. B., and Collins, B. D.: Identifying Physics-Based Thresholds for Rainfall-Induced Landsliding,  
728 *Geophys. Res. Lett.*, 45, 9651–9661, <https://doi.org/10.1029/2018GL079662>, 2018.
- 729 Tiranti, D., Nicolò, G., and Gaeta, A. R.: Shallow landslides predisposing and triggering factors in developing a regional early  
730 warning system, *Landslides*, 16, 235–251, <https://doi.org/10.1007/s10346-018-1096-8>, 2019.
- 731 Trigila, A. and Iadanza, C.: The national landslide inventory, landslide events, impacts and mitigation measures in Italy,  
732 *Landslides Eng. Slopes Prot. Soc. through Improv. Underst. - Proc. 11th Int. 2nd North Am. Symp. Landslides Eng. Slopes*,  
733 2012, 273–278, 2012.
- 734 Varnes, D. J.: *Landslide Hazard Zonation—A Review of Principles and Practice.*, IAEG Comm. Landslides, Paris, 63 pp.,  
735 1984.
- 736 van Westen, C. J., Castellanos, E., and Kuriakose, S. L.: Spatial data for landslide susceptibility, hazard, and vulnerability  
737 assessment: An overview, *Eng. Geol.*, 102, 112–131, <https://doi.org/10.1016/j.enggeo.2008.03.010>, 2008.
- 738 Wu, W. and Sidle, R. C.: A distributed slope stability model for steep forested basins, *Water Resour.*, 31, 2097–2110, 1995.
- 739 Yordanov, V. and Brovelli, M. A.: Comparing model performance metrics for landslide susceptibility mapping, *Int. Arch.*  
740 *Photogramm. Remote Sens. Spat. Inf. Sci. - ISPRS Arch.*, 43, 1277–1284, [https://doi.org/10.5194/isprs-archives-XLIII-B3-](https://doi.org/10.5194/isprs-archives-XLIII-B3-2020-1277-2020)  
741 2020-1277-2020, 2020.
- 742 Yule, G. U.: On the association of attributes in statistics, *Philos. Trans. R. Soc. London. Ser. A, Contain. Pap. a Math. or Phys.*  
743 *Character*, 194, 257–319, <https://doi.org/10.1098/rsta.1900.0019>, 1900.
- 744 Zhao, Z., He, Y., Yao, S., Yang, W., Wang, W., Zhang, L., and Sun, Q.: A comparative study of different neural network  
745 models for landslide susceptibility mapping, *Adv. Sp. Res.*, 70, 383–401, <https://doi.org/10.1016/j.asr.2022.04.055>, 2022.